International Journal on Magnetic Particle Imaging
Vol 9, No 1, Suppl 1, Article ID 2303035, 5 Pages

Infinite Science Publishing

Proceedings Article

A physics-informed deep learning framework in multi-color magnetic particle signal analysis

Jiaming Peng[a] · Guang Jia[b,*] · Xin Feng[c] · Yubo Wang[a] · Liyu Huang[a,*] · Xiaofeng Liang[b] · Qiguang Miao[b] · Kai Hu[d] · Tanping Li[d] · Ying Wang[e] · Li Xi[e] · Hui Hui[c] · Jie Tian[c,*]

[a]School of Life Science and Technology, Xidian University, Xi'an Shaanxi 710071, China
[b]School of Computer Science and Technology, Xidian University, Xi'an Shaanxi 710071, China
[c]CAS Key Laboratory of Molecular Imaging, Institute of Automation, Chinese Academy of Sciences, Beijing, 100190, China
[d]School of Physics, Xidian University, Xi'an, Shaanxi 710071, China
[e]School of Physical Science and Technology, Lanzhou University, Lanzhou, Gansu 730000, China
*Corresponding author, email: gjia@xidian.edu.cn, huangly@mail.xidian.edu.cn, jie.tian@ia.ac.cn

Abstract

Magnetic particle imaging (MPI) is an emerging and highly sensitive imaging method. Multi-color MPI allows simultaneous identification of different materials. Obtaining precise relaxation time is one of the key challenges in achieving multi-colored MPI. In this paper, we propose a physical information based deep learning framework to accurately decompose the mixed signal into the original independent relaxation signals. By transforming the Debye relaxation model into a differential loss function, our network is able to efficiently utilize physical prior information. In simulation experiments with different signal-to-noise ratios and different signal counts, our method shows better performance than the PDCO algorithm. The imaging effect of our algorithm and PDCO algorithm in the presence of multiple materials was evaluated by three-color imaging simulation experiment. In addition, spectral imaging of a digital vascular phantom was simulated by combining a field-free point with homogeneous pulsed excitation. In vascular phantom simulation experiment, our method images blood vessels, metal guidewires, and stents in a single imaging process, showing excellent application potential in cardiac stent surgery.

I. Introduction

Multi-color MPI enables reconstruction of separate images for the catheter and the vessels from the mixed signal [1]. The relaxation mechanisms of magnetization in response to excitation magnetic fields are important features of magnetic nanoparticles (MNPs) [2]. It is possible to obtain a mixed signal with constant Néel and Brownian relaxation time by field-flat phase in pulse excitation. Thus, the relaxation time can be used as a criterion to distinguish different materials in multi-color MPI. However, it's challenging to separate the original multiple relaxation signals from the mixed signal.

In this study, we developed a deep learning framework embedded with physics information to convert the mixed signal to multiple relaxation signals. To embed the physical prior information, we convert the Debye relaxation model into the corresponding partial differential loss. To evaluate the performance of the algorithm, we performed simulation signal decomposition and imaging experiments on our method and PDCO algorithm [3]. The experimental results show that our algorithm shows better performance in both signal decomposition and imaging experiments because it avoids the systematic error caused by discrete representations.

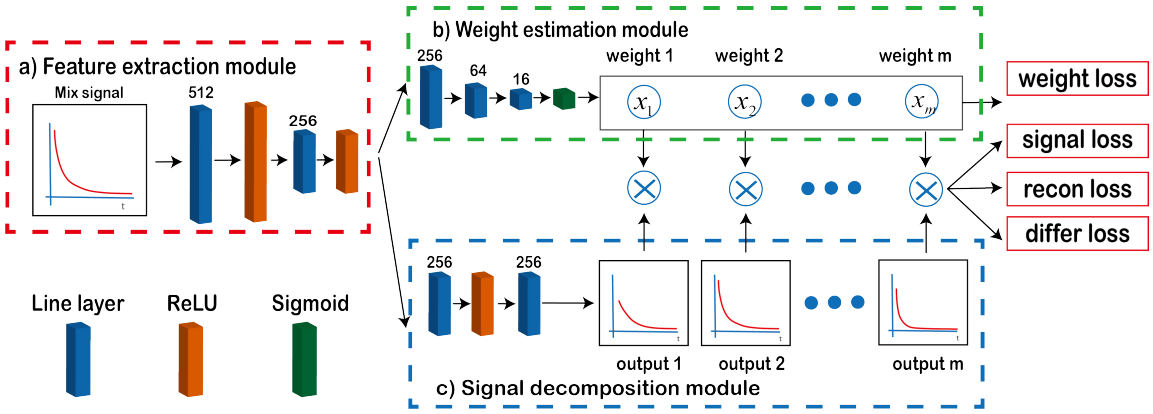

Figure 1: The network architecture of our method.

II. Theory

II.I. Trapezoidal-Waveform Excitation

We simulate decay signal in the field-flat portion under pulse excitation. The magnetization magnitude $M(t)$ in the field-flat phase can be described with relaxation time τ as follow [4]

$$M(t)=M(0)\times e^{-\frac{t}{\tau}}, \tag{1}$$

where $M(0)$ denotes the magnetization when the magnetic field is turned off. Normalize the magnetization, the delay signal can be computed by

$$S_{flat}(t)=\frac{w}{\tau}e^{-\frac{t}{\tau}}\times u(t)+\varepsilon(t), \tag{2}$$

where w denotes the magnitude of the relaxation signal, and $\varepsilon(t)$ denotes the noise in the signal. $u(t)$ is the Heaviside step function.

Considering only one-sided signals and multiple materials, $S_{flat}(t)$ can be approximated as the sum of several discrete relaxation signals

$$S_{flat}(t)\approx\int_{i=1}^{n} w_i' e^{-\frac{t}{\tau_i}}+\varepsilon(t), \tag{3}$$

where $w_i'=\frac{w_i}{\tau_i}$ represents the i-th signal component as a percentage of the total signal with w_i denoting the proportion of the i-th material in the total material. The τ_i denotes the relaxation time of the i-th signal.

II.II. Relaxation physics-informed model

With $f_i=e^{-\frac{t}{\tau_i}}$, we can get its first- and second-order partial differential with respect to t as follows [5].

$$\frac{df_i}{dt}=-\frac{1}{\tau_i}e^{-\frac{t}{\tau_i}}, \tag{4}$$

$$\frac{d^2f_i}{dt^2}=\frac{1}{{\tau_i}^2}e^{-\frac{t}{\tau_i}}, \tag{5}$$

By transforming the Debye relaxation model into differential constraints, a system of equations for describing multiparticle relaxation processes can be given by

$$\int_{i=1}^{n} w_i' f_i+\varepsilon(t)=S_{flat}(t), \tag{6}$$

$$(F_t)^2-F_{tt}F=0, \tag{7}$$

$$c\frac{df_i}{dt}<0, \tag{8}$$

where $F_t=\{\frac{df_1}{dt},\frac{df_2}{dt},\ldots,\frac{df_n}{dt}\}$ is the first-order partial derivative of $F=\{f_1,f_2,\ldots,f_n\}$ with respect to t, and $F_{tt}=\left\{\frac{d^2f_1}{(dt)^2},\frac{d^2f_2}{(dt)^2},\ldots,\frac{d^2f_n}{(dt)^2}\right\}$ is the second-order partial derivative of F with respect to t.

II.III. Physics-informed deep learning framework

To implement the solution of neural networks, we assume multiple signal prototypes $O=\{o_1,o_2,\ldots,o_m\}$, which are the output of the signal decomposition module. o_i and f_j represent the i-th component of O and the j-th component of F, respectively. We define the similarity matrix D of o_i and f_j as their mean square error.

$$cD_{ij}=(o_i-f_j)^2, \tag{9}$$

According to D we can get a new order of O as $\tilde{O}=\{\tilde{o}_1,\tilde{o}_2,\ \ldots,\tilde{o}_m\}$ to minimize the mean squared error of the first n variables of $\tilde{O}$ and F. Thus, we can get a constraint model of the neural network.

$$\sum_{i=1}^{n} x_i\tilde{o}_i+\varepsilon(t)=S_{flat}(t), \tag{10}$$

$$x_i=0\ \ i>n, \tag{11}$$

$$\tilde{O}_t\tilde{O}_t-\tilde{O}_{tt}\tilde{O}=0 \tag{12}$$

$$\tilde{O}_t<0, \tag{13}$$

$\tilde{O}$ is the output of the neural network, $\tilde{O}_t$ is the first-order partial differential of $\tilde{O}$ with respect to t and $\tilde{O}_{tt}$ is the second-order partial differential of $\tilde{O}$ with respect to t.

10.18416/ijmpi.2023.2303035

II.IV. Network architecture and loss function

Our goal is to learn an output space that can represent all possible signal components and a corresponding weight space when the weights of a real signal approximate their corresponding true weights and the weights of non-existent signal components approximate zero.

The specific network architecture is shown in Fig.1. It contains three network modules, which are a feature extraction module composed of two linear layers and two tanh layers, a signal decomposition module for characterizing the signal space of magnetic particles, and a signal estimation module to obtain signal weights. The loss function consists of four loss terms and is defined as

$$\mathscr{L}=\mathscr{L}_{signal}+\mathscr{L}_{weight}+\mathscr{L}_{differ}+\mathscr{L}_{recon}, \tag{14}$$

$\mathscr{L}_{signal}$ denotes the MSE of the independent signal components and the real signal.

$$\mathscr{L}_{signal}=\begin{cases} \left(x_i\tilde{o}_i-\ w_i{}'f_i\right)^2 & i\le n \\ 0 & i>n \end{cases}, \tag{15}$$

$\mathscr{L}_{weight}$ means weight Loss which is given by

$$\mathscr{L}_{weight}=\begin{cases} \left(\tilde{x}_i-w_i{}'\right)^2 & i\le n \\ \left(\tilde{x}_i\right)^2 & i>n \end{cases}, \tag{16}$$

$\tilde{x}_i$ is the i-th output of the weight estimation module. In order to incorporate physical information in our model, we define $\mathscr{L}_{differ}$ as

$$\mathscr{L}_{differ}=\left\|\tilde{O}_t\tilde{O}_t-\tilde{O}_{tt}\tilde{O}\right\|. \tag{17}$$

To resemble the constraint signal with the input signal, we define reconstruction loss as follows

$$\mathscr{L}_{recon}=\left\|\sum_{i=1}^{n}x_i\tilde{o}_i-\sum_{i=1}^{n}w_i{}'f_i\right\|. \tag{18}$$

III. Materials and Methods

III.I. Data Simulation

Regardless of the effect of convolution, we simulate based on (**??**) and the proportions of individual materials at a certain point.

we constructed 1000 data with 6 different signal-to-noise ratios from 1 dB to 30 dB and 9 different signal component counts from 2 to 10 as training data. We constructed 200 data with 6 different signal-to-noise ratios from 1 dB to 30 dB and 7 different signal component counts from 2 to 8 as test data.

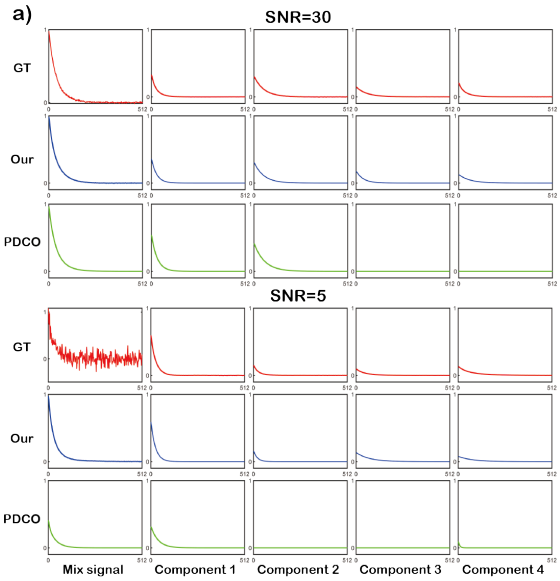

Figure 2: Signal decomposition experiments: Signal decomposition experiment with a signal-to-noise ratio of 5dB and 30 dB. GT denotes the ground truth of the original multiple relaxation signals.

III.II. Training details and comparison algorithms

Our model was trained in Ubuntu 20.04 with Intel® Core™ i5-10400F CPU @ 2.90GHz and GeForce RTX 3080. Before testing, we trained a total of 60 epochs, each with 500 data per epoch.

We compare algorithm performance with PDCO algorithms that apply non-negativity constraints and L1 regularization. The linearly constrained convex optimization problem solved by PDCO is assumed to be of the following form:

$$min_{\mathbf{w},\mathbf{r}}\ \lambda_1\|\mathbf{w}\|_2^1+\frac{1}{2}\lambda_2\|\mathbf{w}\|_2^2+\frac{1}{2}\|\mathbf{r}\|_2^2, \tag{19}$$

$$\mathrm{K}\mathbf{w}+\mathbf{r}=S_{flat}, \tag{20}$$

$$\mathbf{w}>0, \tag{21}$$

Where K is the discrete Laplace transform consisting of $K_{j,h}=e^{-\frac{t_j}{\tau_h}}, h=1,2,\ldots m, j=1,2,\ldots,l$ and τ_h is the h-th of preset relaxation time. In this work, we set $\lambda_2=1$ which is the same as default settings of PDCO and $\lambda_1=\lambda_2$.

III.III. Evaluation Metrics

In this work, mean absolute error (MAE) is used to evaluate differences in performance between methods. MAE is defined as

$$MAE\left(\tilde{O},F\right)=\sum_{i=1}^{m}\sum_{t=0}^{l}\frac{\left|x_i\tilde{o}_i(t)-\ w_i{}'f_i(t)\right|}{ml}, \tag{22}$$

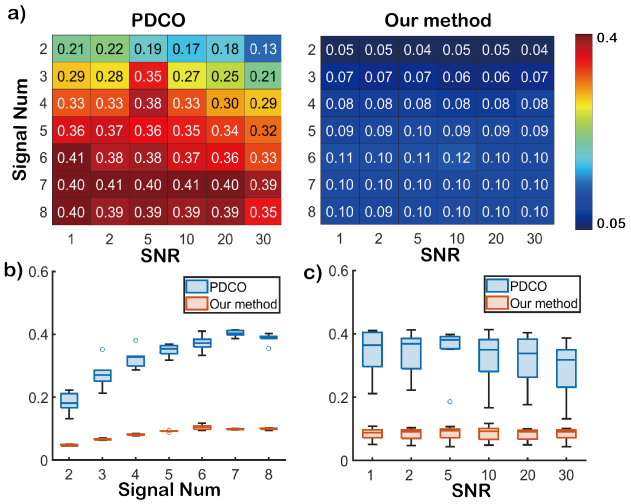

Figure 3: MAE of signal decomposition simulation experiment. a) MAE heatmap of PDCO and our method. b) different number of signal components with signal-to-noise ratio set of 5dB. c) different signal-to-noise ratio with signal components number of 4.

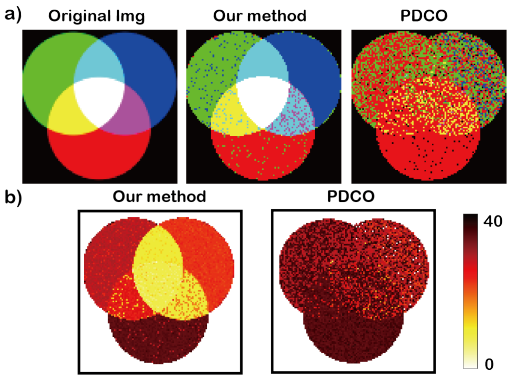

Figure 4: Three-color imaging simulation experiment. a) Imaging results of our method and PDCO. b) MAE distribution image of relation time calculated by our method and PDCO

Given the characteristics of exponentially attenuated signals, weak signals after attenuation will not be considered. A control function is designed to filter weak signals and balance the error of smaller signals.

$$G(f_i)=\begin{cases} 1 & f_i(t)>\varphi \# \# \\ 0 & f_i(t)\le\varphi \end{cases}, \tag{23}$$

$$MAE\left(\tilde{O},F\right)=\frac{1}{m}\sum_{i=1}^{m}\sum_{t=0}^{l}G(F)\frac{\left|x_i\tilde{o}_i(t)-w_i{}'f_i(t)\right|}{f_i(0)\sum_{t=1}^{l}G(f_i)}, \tag{24}$$

$f_i(0)$ represents the value of the signal at 0.

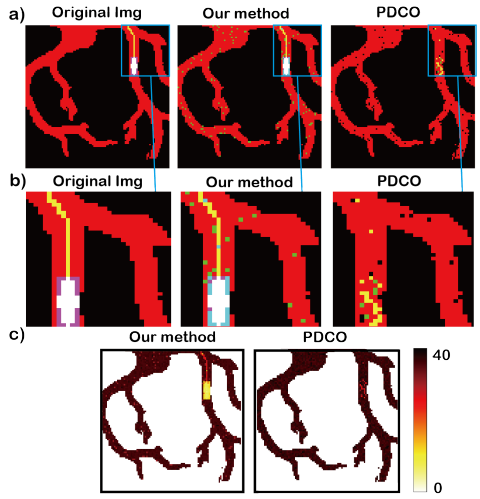

Figure 5: Digital vascular phantom experiment. a) Imaging results of our method and PDCO. b) Local details of imaging results. c) MAE distribution image of relation time calculated by our method and PDCO

IV. Results and Discussions

We compare the performance of our method with PDCO under different signal-to-noise ratios (Fig. 2). At a signal-to-noise ratio of 30dB and 5dB, the MAE of our method is 0.22 and 0.26 lower than that of PDCO, respectively.

As shown in Fig.3 a) the mean standard error of our method is three times smaller than the mean standard error of PDCO. Fig.3 b) and c) show that the variance of our method is 14 times smaller than the variance of PDCO.

In addition, we designed a three-color imaging simulation experiment to verify the performance of our method in multi-color imaging.

According to Fig 4 a), red, blue and green refer to different magnetic particle materials with relaxation times of 20, 40, and 60, respectively. A mixture of three primary colors represents the locations where multiple classes of magnetic nanoparticles are present in this experiment.

As shown in Fig.4 a), our method has an accuracy of 92.67% for three-color imaging simulation experiment, which is 45.49% higher than PDCO. Fig 4 b) shows that our method for MAE on relaxation time in three-color imaging simulation experiment is 6.87 lower than MAE for PDCO

The relaxation spectral imaging of a digital vascular phantom was simulated to show demonstrate imaging results in cardiac stent surgery. The experiment used the same experimental setup as the three-color experiment, with three colors representing blood vessels, metal guidewires and stent.

As shown in Fig.5, our method provides a clear image of the digital vascular phantom, showing the distribution of multiple materials in the mimicry.

10.18416/ijmpi.2023.2303035

V. Conclusions

Our method shows excellent performance and potential in multicolor MPI. However, the model still has the following points that can be improved.

1. After training, less than ten percent of the output nodes used to characterize the signal space are activated, so we need to find a way to characterize the signal space more comprehensively.
2. More prior information can be introduced to improve network performance, such as the Langevin function.

Author's statement

This work was supported by the National Natural Science Foundation of China (Grant number 82227802). Conflict of interest: Authors state no conflict of interest. Informed consent: Not applicable. Ethical approval: Not applicable.

References

[1] Rahmer J, Wirtz D, Bontus C, et al. Interactive magnetic catheter steering with 3-D real-time feedback using multi-color magnetic particle imaging[J]. IEEE transactions on medical imaging, 2017, 36(7): 1449-1456.

[2] C. Lu, L. Han, J. Wang et al., "Engineering of magnetic nanoparticles as magnetic particle imaging tracers," Chem. Soc. Rev., vol. 50, no. 14, pp. 8102-8146, 2021.

[3] Berman P, Levi O, Parmet Y, et al. Laplace inversion of low-resolution NMR relaxometry data using sparse representation methods[J]. Concepts in Magnetic Resonance Part A, 2013, 42(3): 72-88.

[4] Knopp T, Buzug T M. Magnetic particle imaging: an introduction to imaging principles and scanner instrumentation[M]. Springer Science & Business Media, 2012.

[5] Croft L R, Goodwill P W, Konkle J J, et al. Low drive field amplitude for improved image resolution in magnetic particle imaging[J]. Medical physics, 2016, 43(1): 424-435.

[6] Lu L, Jin P, Pang G, et al. Learning nonlinear operators via DeepONet based on the universal approximation theorem of operators[J]. Nature Machine Intelligence, 2021, 3(3): 218-229.

